Supplementary Material for the article:

Possible Shallow Tectonic Tremor Signals Near the Deformation Front in Central Cascadia

Zoe Krauss[1], William S.D. Wilcock[1], Kenneth C. Creager[2]

[1]School of Oceanography, University of Washington, Seattle, WA

[2]Department of Earth and Space Sciences, University of Washington, Seattle, WA

This document contains:

Figures S1-16

Tables S1-4

Text S1

Text S2

Figures S2-3 and Tables S1-2 are embedded within Text S1. Figure S4 is embedded within Text S2. All other supplemental figures (Figures S1 and S4-16) are listed in the order cited in the manuscript, followed by the additional supplemental tables (Tables S3-4).

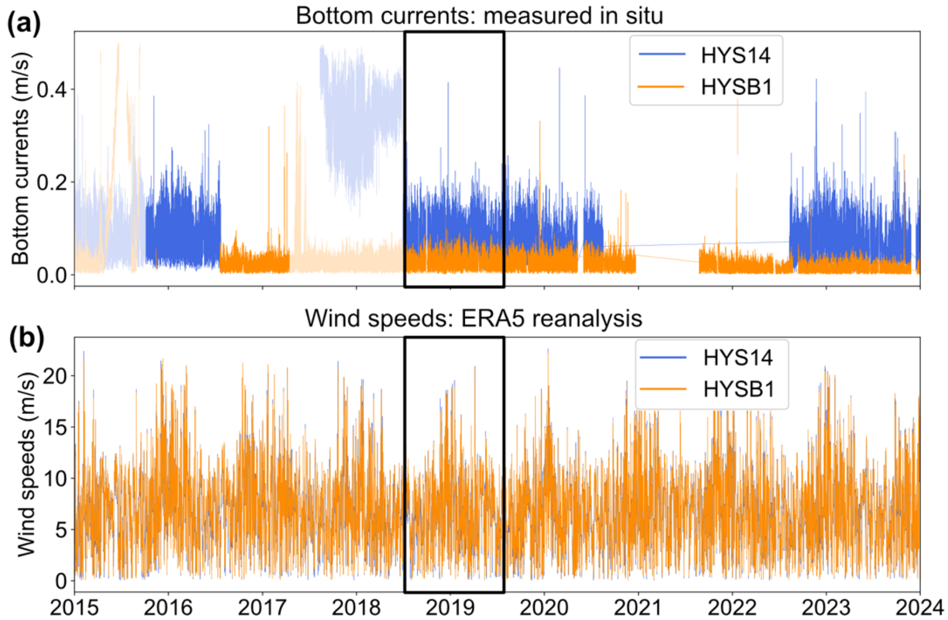

Figure S1. *Environmental data used to compare to seismic time series.* ***(a)*** *Hourly bottom currents measured in situ by cabled instruments at the Hydrate Ridge (HYS14) and Slope Base (HYSB1) sites. Data is shown as hourly medians. Periods of bad data quality are shown with paler colors.* ***(b)*** *Hourly wind speeds from ERA5 climate reanalysis for the two sites. The period we use for our analysis is outlined with a black rectangle in both subplots.*

Text S1– Tuning of T-phase and Ship Noise Classification

We randomly selected a subset of 200 STA/LTA detections between July 2018-July 2019 for each of the OOI stations, HYS14 and HYSB1. We visually inspected the waveforms and spectrograms of each of these detections and labeled them as one of three categories: clear T-phases, pure ship noise with no other overlying signals, or mixed signals, which include both T-phases, ship noise, and other background signals including marine mammal calls.

The detection subset for station HYS14 included 52 clear T-phases, 16 ship noise detections, and 132 mixed detections (Figure S2, Table S1). The detection subset at HYSB1 included fewer clear T-phase arrivals, 30 overall, with most T-phases overlain with significant other noise sources (Figure S3, Table S2). There was also a higher proportion of detections on pure ship noise, 67 overall, which present in a variety of ways, from more widely spaced strong spectral bands (similar to Figure S2c) to many closely spaced bands (e.g. Figure S3c).

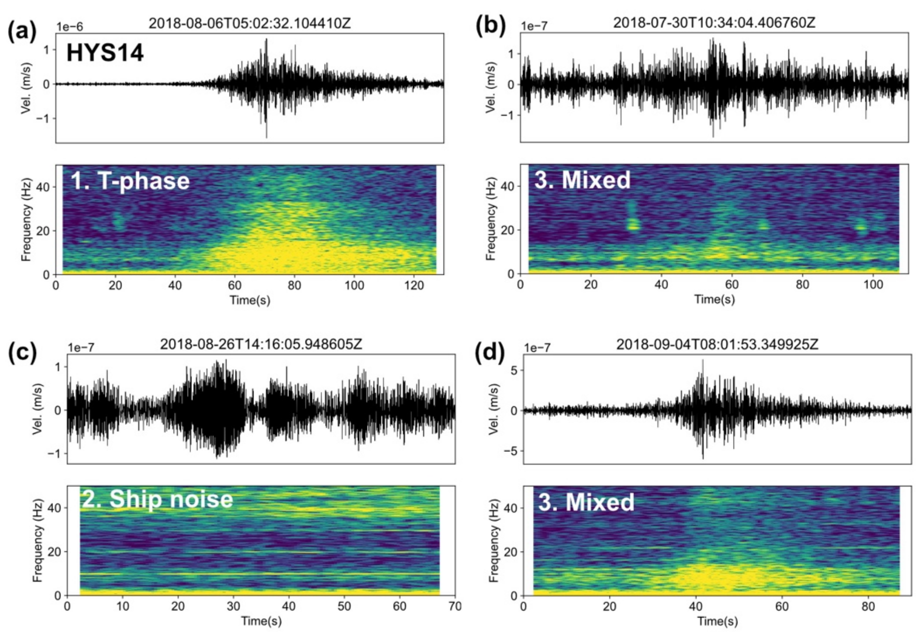

Figure S2. *Examples of manually classified STA/LTA detections on the HYS14 station, channel HHN. Waveforms are filtered from 3-10 Hz. All subplots follow the format of Figure 2a-b.* ***(a)*** *Clear T-phase* *with minimal background noise.* ***(b)*** *T-phase overlain with ship noise and marine mammal calls.* ***(c)*** *Detection on ship noise only.* ***(d)*** *T-phase overlain with ship noise.*

HYS14	Number in subset	Classified as T-phase	Classified as ship noise
1. Obvious T-phases	52	40	3
2. Obvious ship noise	16	4	12
3. Mixed/Other	132	77	21

Table S1. *Classifications on the subset of 200 detections from HYS14, and results from T-phase and ship noise classification.*

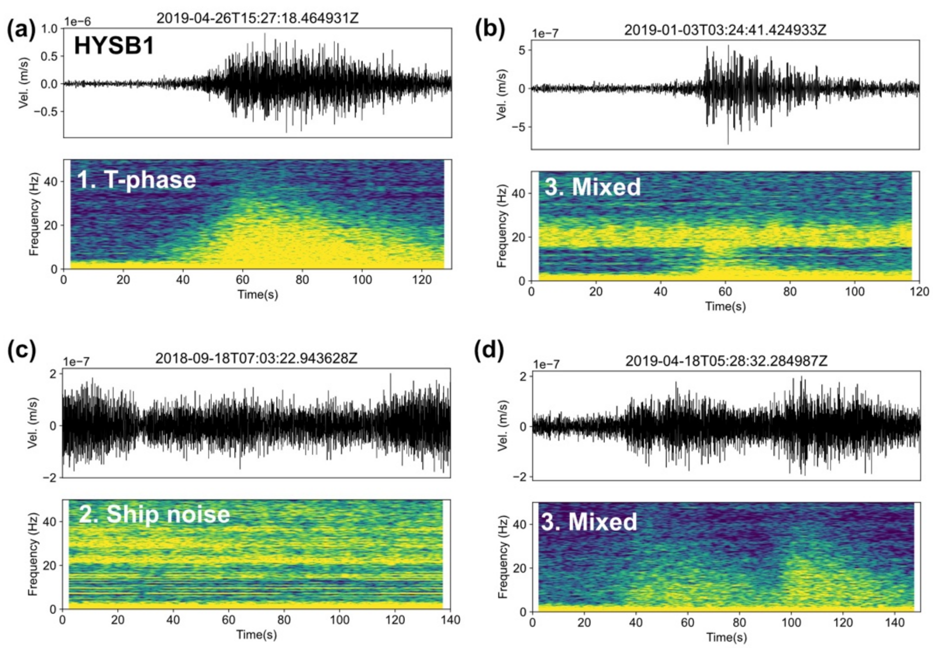

Figure S3. *Examples of manually classified STA/LTA detections on the HYSB1 station, channel HHN. Waveforms are filtered from 3-10 Hz. All subplots follow the format of Figure 2a-b.* ***(a)*** *Clear T-phase with minimal background noise.* ***(b)*** *T-phase overlain with ship noise and saturate background noise in* *the marine mammal call band, ~18-24 Hz.* ***(c)*** *Detection on ship noise only, with closely spaced spectral bands.* ***(d)*** *T-phase or earthquake arrival with multiple phase arrivals or multiple T-phases.*

HYSB1	Number in subset	Classified as T-phase	Classified as ship noise
1. Obvious T-phases	30	17	12
2. Obvious ship noise	67	21	57
3. Mixed/Other	103	50	54

Table S2. *Classifications on the subset of 200 detections from HYS14, and results from T-phase and ship noise classification.*

We iteratively tuned the filtering and peak-picking parameters used to classify detections as T-phases and ship noise. For T-phase identification, we favored conservative parameters that led to more false negatives than false positives, to ensure we were not discarding any potential tremor signals. Our finalized approach correctly identifies the majority of clear T-phases in both random subsets, 77% in the HYS14 subset and 57% in the HYSB1 subset (Tables S1 and S2). T-phases in the HYSB1 subset more frequently appeared as broader signals with less of a prominent peak (Figure S3a), leading to poorer classification performance. Because HYS14 records more T-phases overall, we prioritized classification performance on that station. Many of the mixed signals in both station subsets were classified as including T-phases, which we visually verified.

Our classification parameters for ship noise also identify the majority of obvious detections on ship noise in both random subsets, 75% in the HYS14 subset and 85% in the HYSB1 subset (Tables S1 and S2). But, because we found that ship noise frequently occurs within detections that also include other signals, we did not use the ship noise classifier to discard detections in the end. We found that identification of ship noise in the form of spectral banding was difficult to tune using only one set of peak-picking parameters because it presents in many ways, including both widely and narrowly spaced spectral peaks (e.g., Figure S2c and S3c).

Text S2– Application of method to OBSs from the NoMelt experiment

We apply our approach of single-station STA/LTA triggering and subsequent detection classification to three broadband OBSs from the NoMelt experiment in the central Pacific: station codes B05, B24, and B24, which are approximately evenly distributed throughout the 600 km x 400 km aperture of the experiment (Lin et al., 2016). Stations B05, B25 and B24 are deployed at -5197, -5110, and -5158 m water depths, respectively. All stations sample at 50 Hz and we use the BH1 channels for our analysis. We analyze all available data, approximately one year per station (Figure S4). Due to the distance of the experiment from active tectonic structures, we do not expect the OBSs to record any tectonic tremor signals.

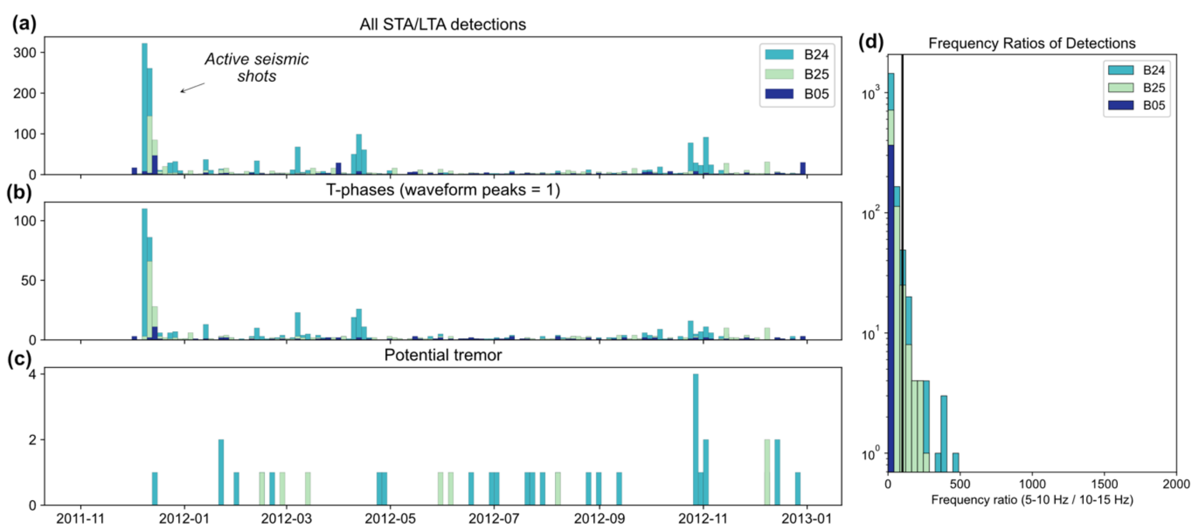

Figure S4. *Same as Figure 5, but for three OBSs from the NoMelt experiment in the central Pacific. The detection peak that is due to an active seismic experiment is annotated in (a). Note that (c) is not shown in log scale due to the small number of detections.*

STA/LTA triggering identifies 365, 870, and 1694 emergent signals on stations B05, B25, and B24, respectively (Figure S4a). The peak in detections at the start of the deployment is due to airgun activity from the accompanying active seismic experiment. The F_{LH} values of all detections do not exceed 500 (Figure S4d), and display a more limited distribution than both the

Hikurangi and OOI datasets (Figures 4b and 5d); this highlights the lack of tectonic tremor-like signals in the dataset. For each of the stations, ~30% of detections have one peak in their smoothed waveforms and are classified as T-phases (Figure S4b). By requiring more than one peak in the smoothed waveform and $F_{LH} > 100$, we classify 0, 8, and 29 of the total emergent signals as potential tectonic tremor signals for stations B05, B25, and B24, respectively (Figure S4c). Visual inspection of these signals shows that for station B25, eight of the detections are regional T-phases (similar to Figure S9a), three are bottom-current generated harmonic tremor (similar to Figure S8), and one contains SDEs (similar to Figure S9b). For station B24, 23 of the detections are regional T-phases, and the remainder are bottom-current generated harmonic tremor or apparent instrument noise.

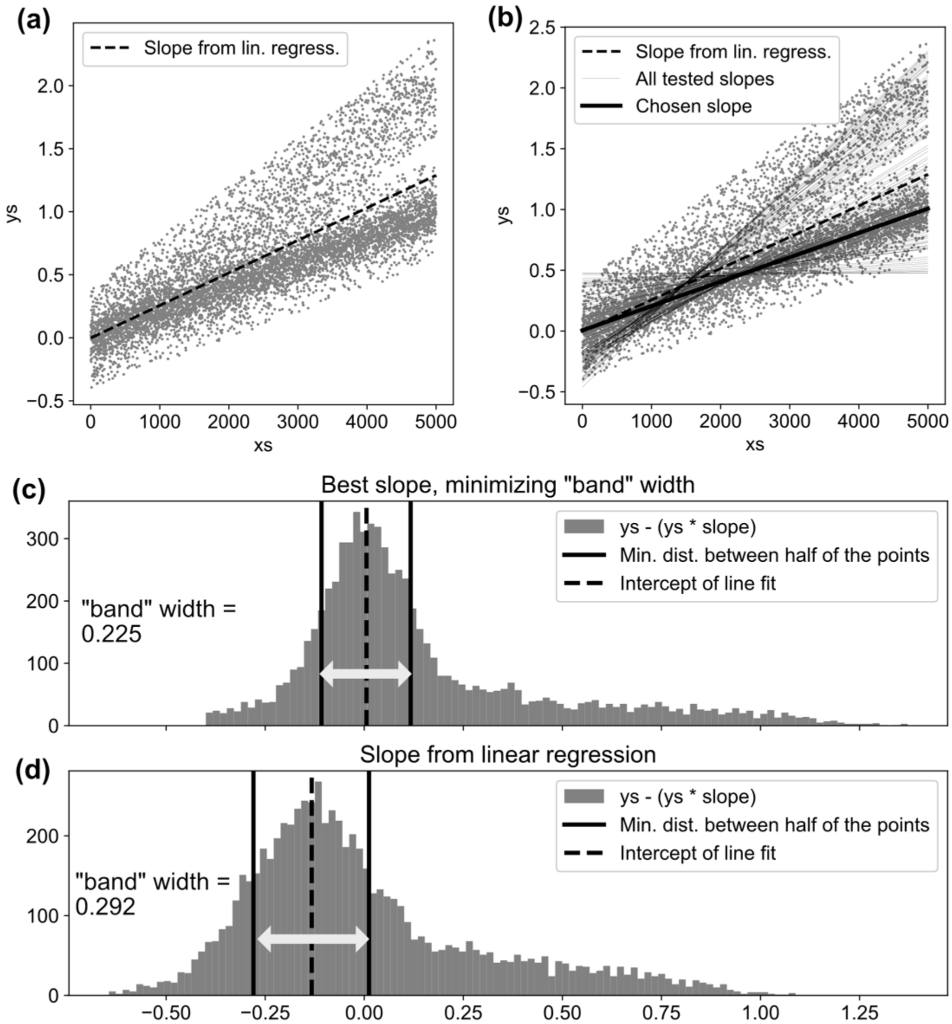

Figure S5. *Illustration of the line-fitting method used for environmental data (Section 3.1), designed to avoid the influence of outliers. Here, we compare the difference between line fits from simple linear regression and our approach, for an asymmetric synthetic distribution.* ***(a)*** *Synthetic data distribution showing the line fit calculated using linear regression.* ***(b)*** *Synthetic data distribution comparing the linear regression fit (dashed line), our chosen fit (bold line), and all of our tested slopes (fine lines). It is clear that our chosen fit better prioritizes the greatest density of data points. Our approach chooses the line that gives the center of the narrowest band enclosing half the points in the y-direction, as illustrated in* ***(c)****: to calculate "band" width for a given slope, we first calculate the residuals between our data and a line with that slope (plotted as a histogram). We then find the edges of the smallest band that encloses half of the points in the overall distribution (solid horizontal lines). The width of this band is shown using a white arrow. We calculate this band width for each tested slope, and choose the slope that minimizes the band width. The intercept used for the resulting line fit is taken as the mean of the values within the band.* ***(d)*** *Same as (c), but showing the band width for the slope from the linear regression line fit instead. For distributions with a clear hinge point, we perform this same approach for each half of the distribution (above and below the hinge) but require that one end of the fitted line intersects the hinge point.*

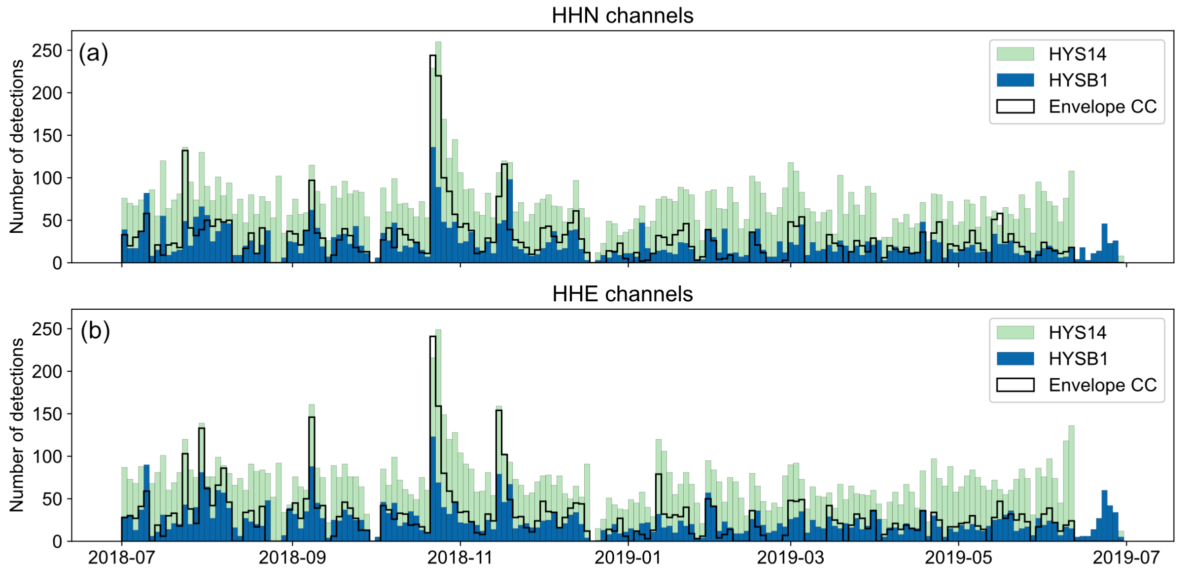

Figure S6. *Comparison of emergent signal detection methods for July 2018-July 2019 for* ***(a)*** *the HHN and* ***(b)*** *HHE channels. On each plot, colored histogram bars show the number of emergent detections, with bin sizes of 2 days, detected on the Hydrate Ridge (HYS14) and Slope Base (HYSB1) OOI stations using STA/LTA on the HHN channels. The unfilled black histogram overlain shows the number of detections from envelope cross-correlation between the two stations. The highest peak in detections corresponds to regional T-phase arrivals from a swarm of earthquakes on the Nootka fault zone in October 2018.*

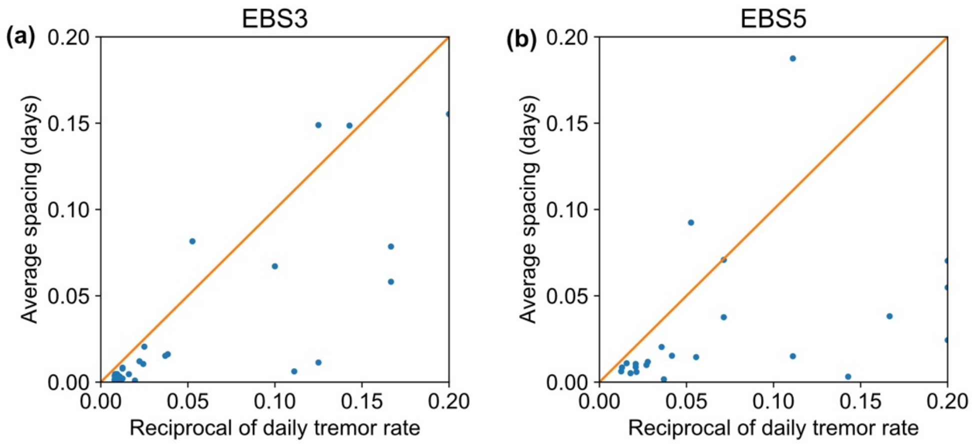

Figure S7. *Relationship between the reciprocal daily tremor rate of STA/LTA detections and the daily average temporal distance between STA/LTA tremor detections and the detections of Todd et al. (2018), for **(a)** the EBS3 station and **(b)** the EBS5 station. In both subplots, each blue point corresponds to one day from September-November 2014. We would expect a 1:1 relationship (orange line) if the temporal spacing between STA/LTA and Todd et al. (2018) detections only improves due to overall more detections. However, for both stations, we see that the distribution falls below the 1:1 line. This indicates that the improved timing is instead due to better detection sensitivity.*

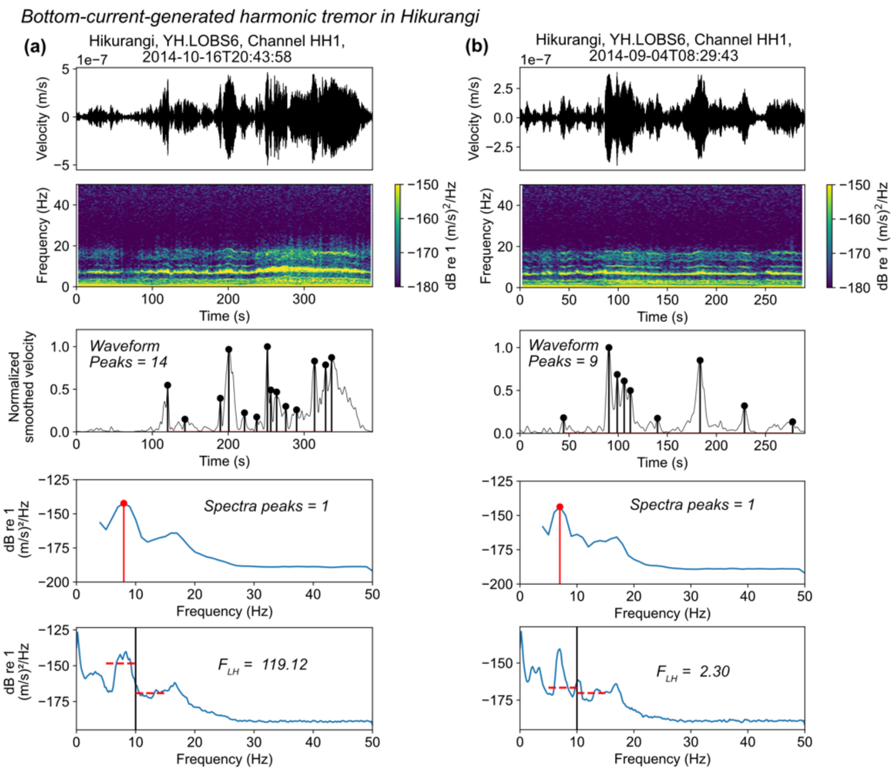

Figure S8. *Examples of bottom current-induced tremor detected by STA/LTA triggering on Hikurangi station LOBS6 using the same format as Figure 2..*

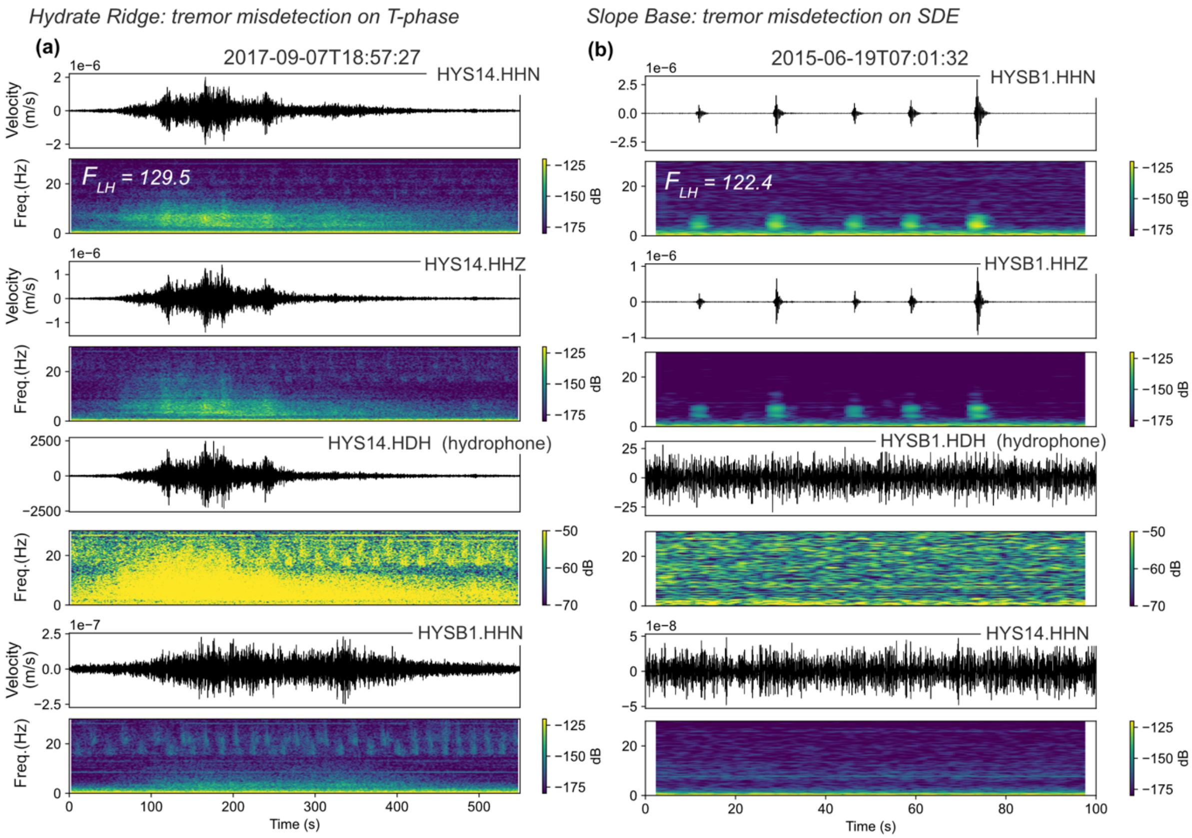

Figure S9. *Examples of potential tremor detections (Figure 6a) that were found by visual detection to be inconsistent with tectonic tremor.* ***(a)*** *Misdetection on a T-phase at Hydrate Ridge. From top to bottom, each waveform-spectrogram pair set shows the record from the Hydrate Ridge horizontal channel, the Hydrate Ridge vertical channel, the Hydrate Ridge hydrophone, and the Slope Base horizontal channel. All waveforms are filtered from 3-10 Hz. The F_{LH} value of the detection, 129.5, is annotated on the HHN spectrogram. The window start time is the title of the first subplot.* ***(b)*** *Misdetection on a sequence of short duration events (SDEs) at Slope Base. The subplot format follows (a) except the plots are for the opposite stations.*

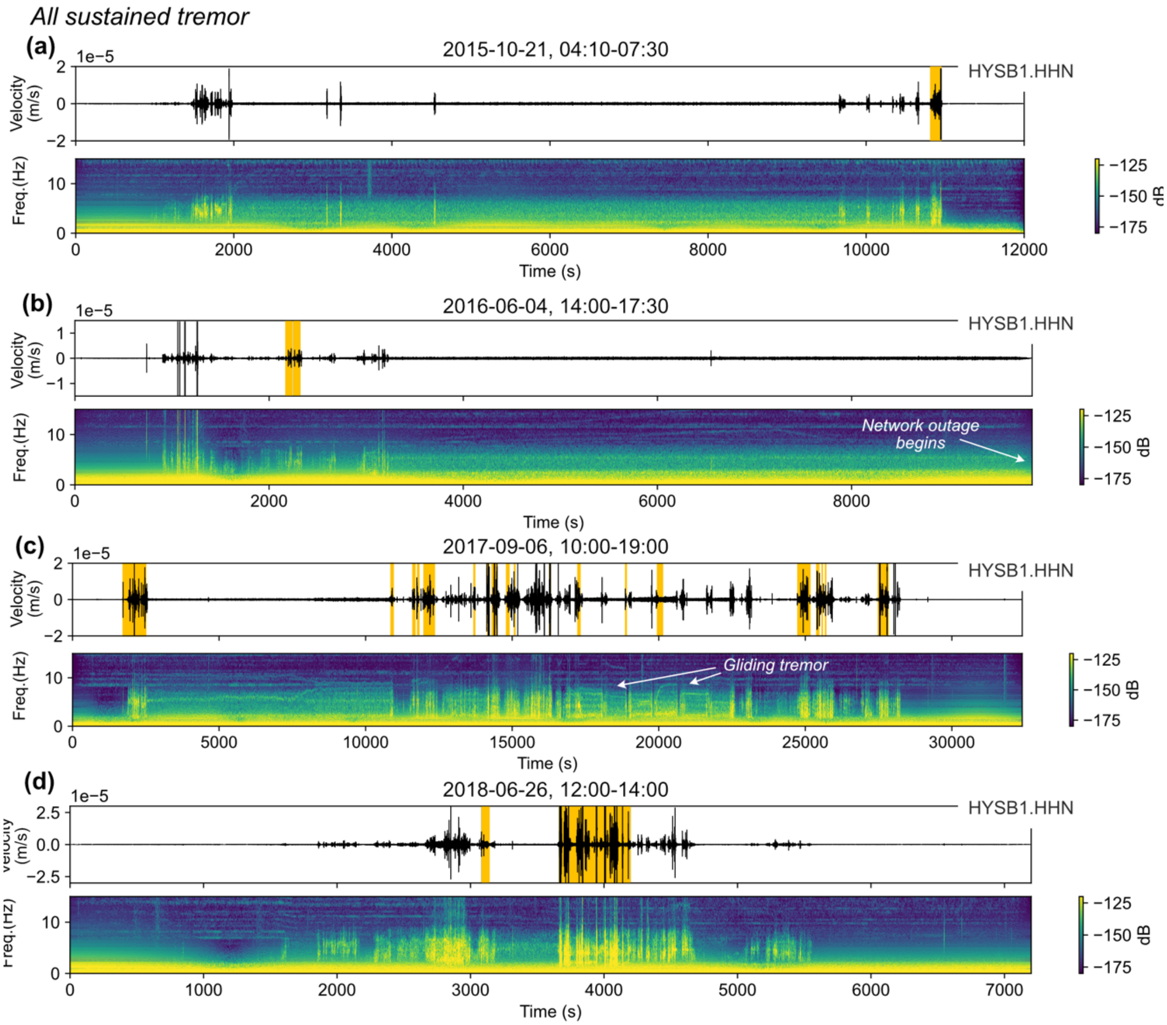

Figure S10. *Full intervals for all periods of sustained tremor, shown only for the Slope Base horizontal channel. Note differing time axes. All waveforms are clipped to emphasize the tremor-like signal.* ***(a-d)*** *Start and end time of each window is noted in the subplot titles. All waveforms are filtered from 3-10 Hz and overlain by yellow rectangles during the times of our detections (Figure 6a). Gliding tremor seen during the 2017 period, as discussed in the text, is marked in (c).*

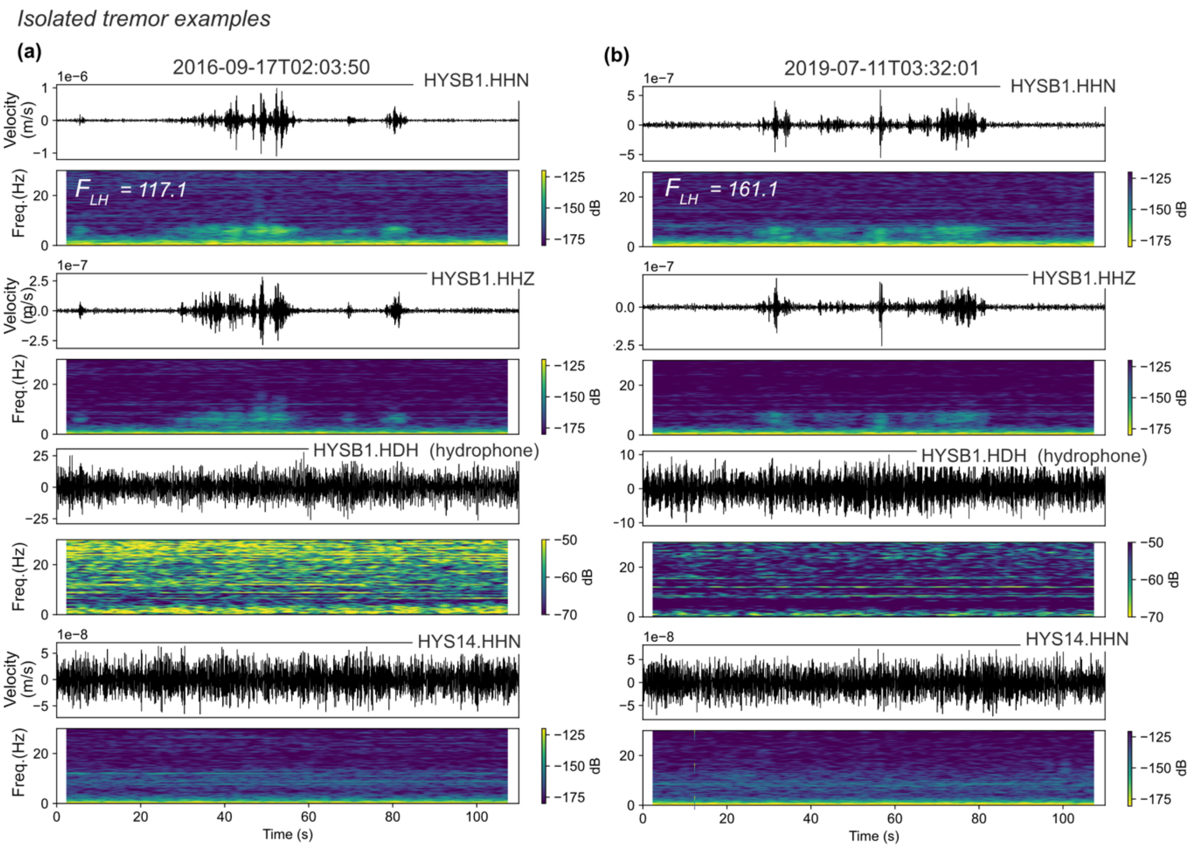

Figure S11. *Examples of isolated tremor signals detected at Slope Base. Figure format follows Figure S9b, with all waveforms filtered from 3-10 Hz.*

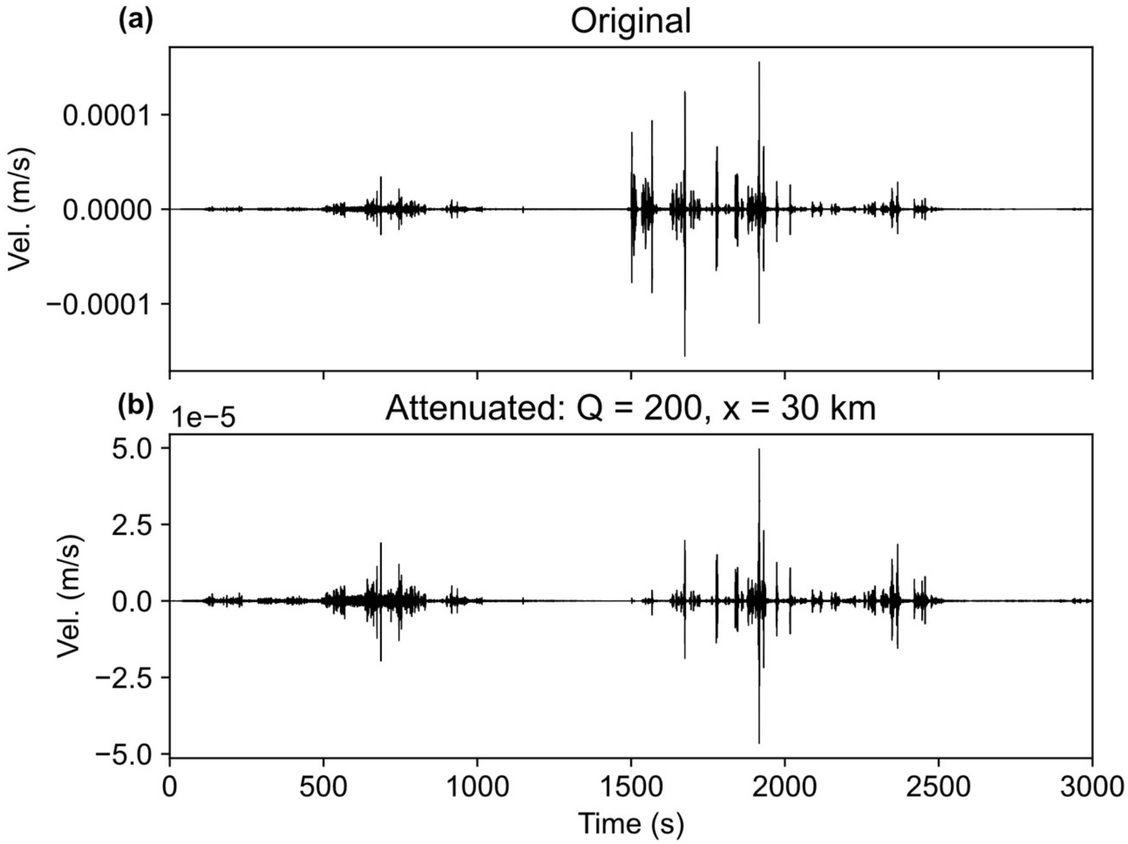

Figure S12. *Waveform attenuation of long-duration tremor signal on 2018-06-26 on station HYSB1 channel HHN.* ***(a)*** *50-minute waveform, from 12:36-13:26, filtered from 3-10 Hz.* ***(b)*** *Same waveform as (a), but after attenuation via Azimi's relation (Azimi, 1968), assuming a distance of 30 km following typical downdip tremor depths (Wech, 2010), an S-wave velocity of 4.5 km/s, and a Q_S value of 200 with a dominant frequency of 2 Hz, following regional studies (e.g. Sweet et al., 2019).*

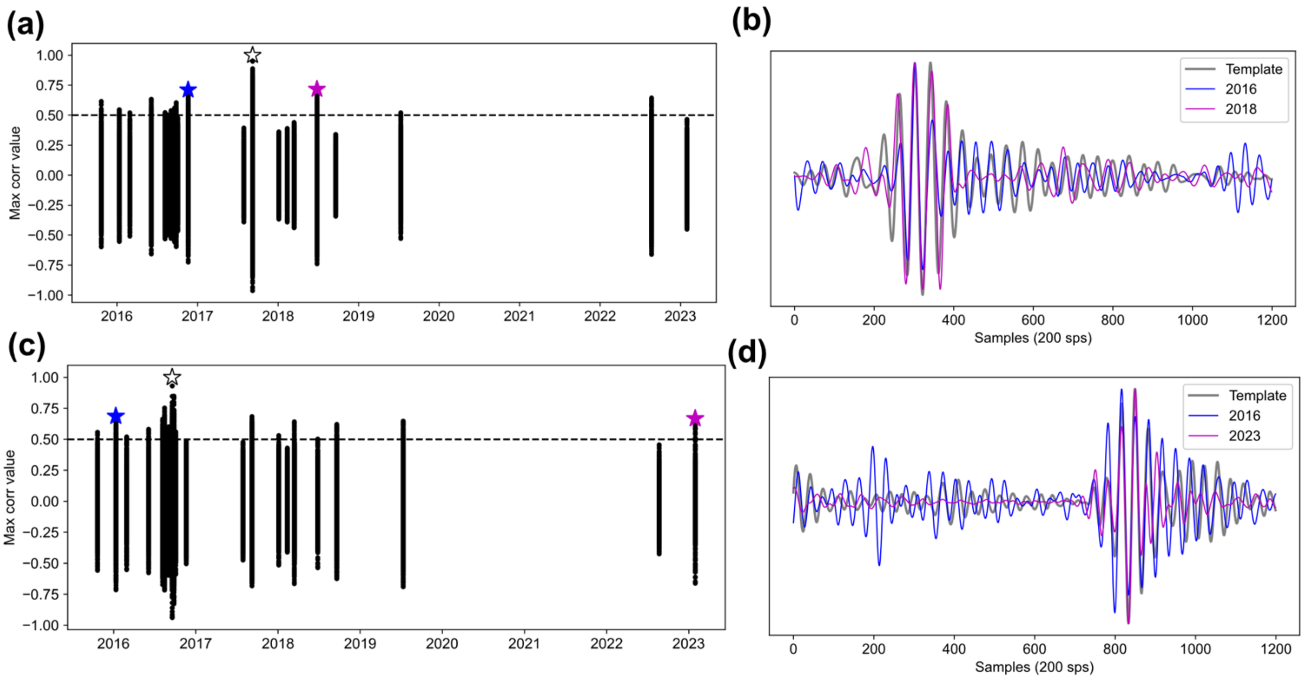

Figure S13. *Two examples of 6-s waveforms within tectonic tremor-like signals at HYSB1 that are highly similar to waveforms at other times. We split the entire tremor dataset (5570 s total) into 6-s "templates" with a step of 0.5 s, following the approach of Brown et al. (2008), and we find many more examples of high correlation than we present here.* ***(a)*** *Cross-correlation values between a 6-s window taken from 2017 (white star, referred to as the "template") and all other times of tremor detection, on HYSB1 channel HHN, bandpass filtered from 3-10 Hz. There are many times during tremor episodes in other years that the template correlates at values > 0.5, which is higher than the typical threshold required to identify LFEs (e.g., Shelly et al., 2007). A cross-correlation value of 0.5 is marked with the dashed horizontal line. The times of the waveforms shown in (b) are marked with blue and magenta stars.* ***(b)*** *6-s waveforms of the template shown in (a) (gray), overlain by the waveforms from times of high cross-correlation in 2016 (blue) and 2018 (magenta). All waveforms are normalized by their maximum value.* ***(c)*** *Same as (a) but for a 6-s template taken from 2016.* ***(d)*** *Same as (b) but for the time windows corresponding to (c).*

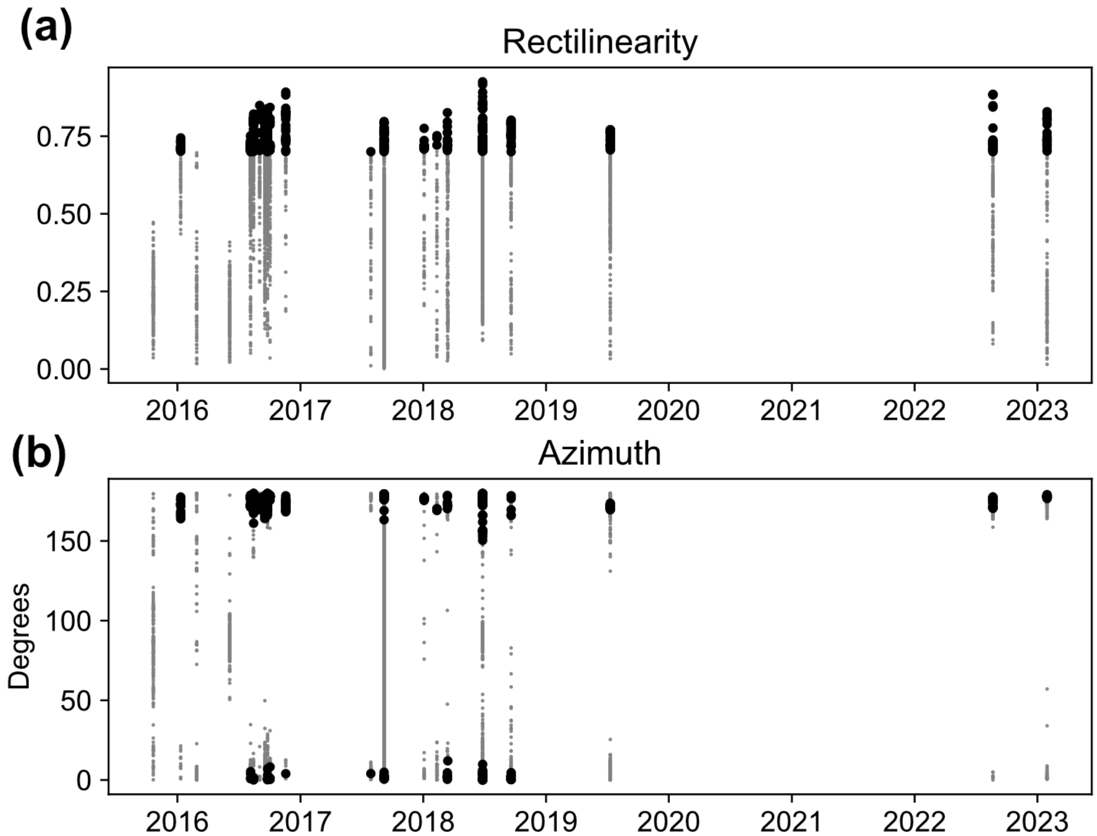

Figure S14. *Results of particle motion analysis performed on the entire tectonic tremor-like dataset (5570 s total), on 6-s sliding windows at a step of 0.5 s using the approach of Flinn (1965). Three-component waveforms from HYSB1 are first bandpass filtered from 3-10 Hz.* ***(a)*** *Values of rectilinearity of each 6-s window shown as light gray points over time. Rectilinearity ranges from 0-1, with 1 corresponding to pure body waves. 6-s windows that have rectilinearity exceeding 0.7 are shown as thicker black circles.* ***(b)*** *As in (a), but showing corresponding azimuth values of each 6-s window over time. Values from windows with rectilinearity > 0.7 are shown as thicker black circles. The median azimuth from this high-rectilinearity subset is 175.8°, with a standard deviation of 5.3°.*

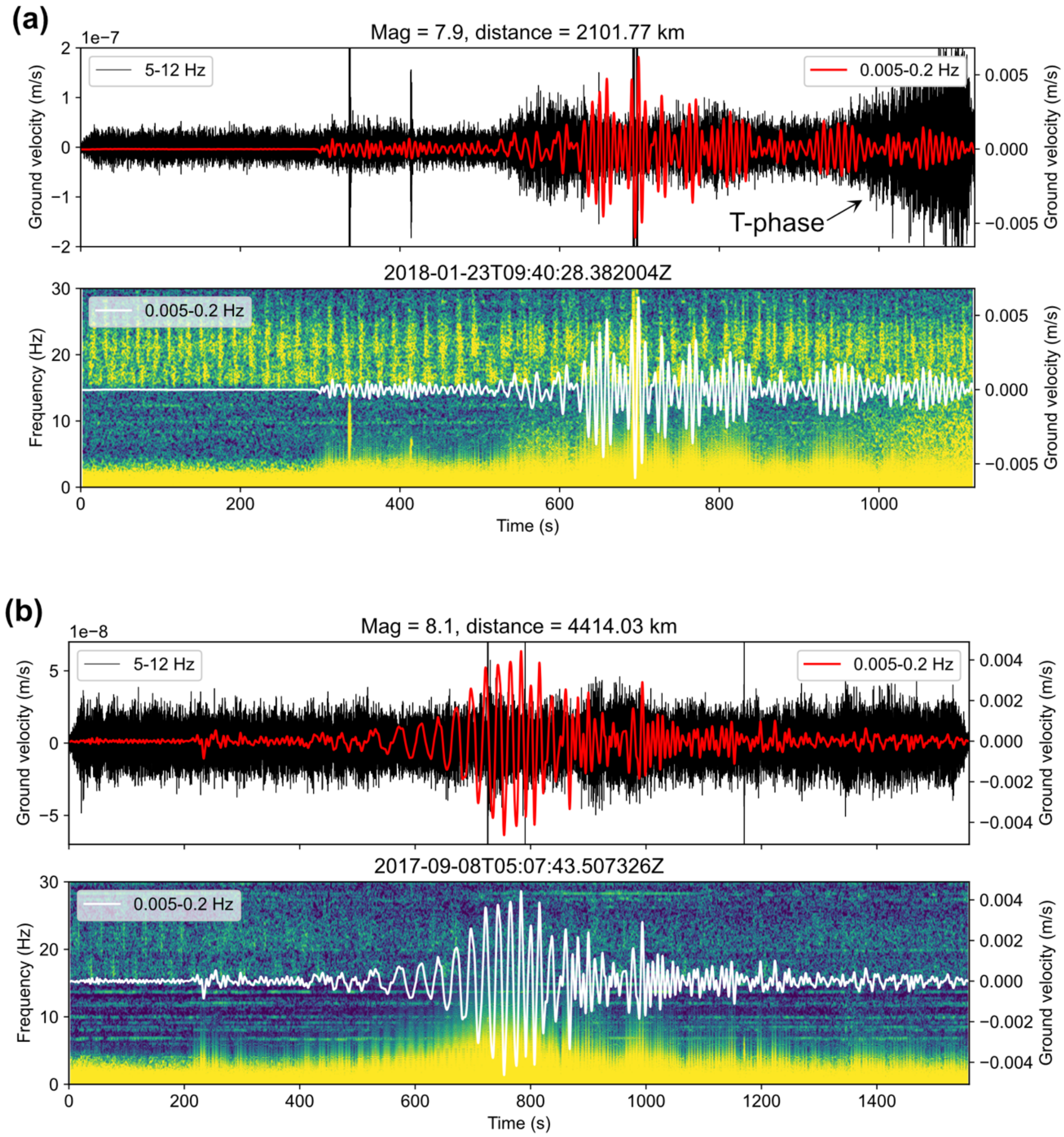

Figure S15. *Seismic waveforms and spectrograms for the two time periods most likely to include dynamically triggered tremor, centered around the surface wave arrivals with the highest amplitudes during the study period, at station HYSB1 channel HHN. The magnitude and distance of the earthquake source and the start time of the window are listed in the subplot titles. The waveform plots show the 5-12 Hz band, which is expected to contain triggered tremor, in black, with the surface wave arrivals, at 0.005-0.2 Hz, overlain in red. The spectrograms are overlain with the same surface wave arrival signal but in white.* ***(a)*** *Surface wave arrivals from an earthquake in Alaska. The T-phase from the earthquake arrives towards the end of the window.* ***(b)*** *Surface wave arrivals from an earthquake in Mexico. Both (a) and (b) show energy in the tremor band (5-12 Hz) increasing with the surface wave arrivals, but this energy does not appear to be modulated by the surface wave peaks, as expected for triggered tremor. However, examination of these same events recorded at other buried broadband OBS elsewhere on the heavily sedimented Cascadia margin, including the broadband station at Hydrate Ridge and a broadband station offshore Vancouver Island that is not expected to exhibit triggered tremor (McGuire et al., 2018), show a similar signal in the 5-12 Hz band. This is not observed at an unsedimented broadband instrument on*

Axial Seamount or short period stations at Hydrate Ridge. These observations, alongside the lack of signal modulation by the surface wave peaks, suggest that the signal at 5-12 Hz is not triggered tremor, but instead may be a response of the seismometer installation to strong shaking.

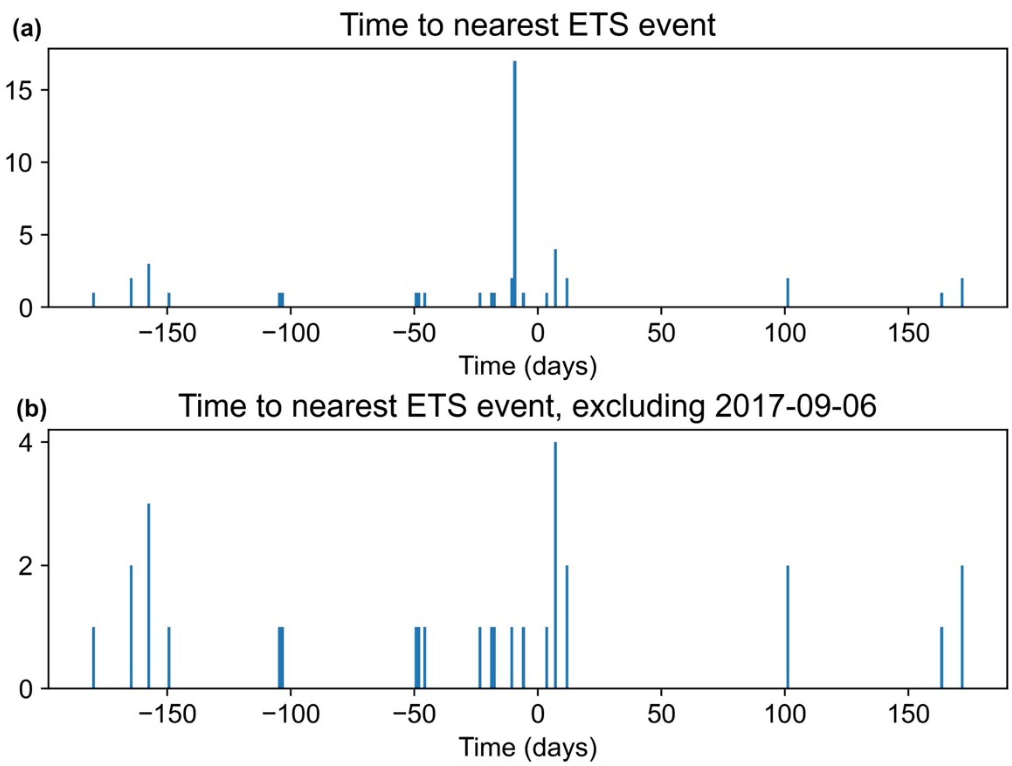

Figure S16. *Histograms showing the time difference between validated tremor detections at HYSB1 and the nearest downdip tremor detections in deep Cascadia, as detected by the Pacific Northwest Seismic Network (Wech, 2010), between 44°N and 45°N and west of 123.5°W (Figure 6b). Negative values indicate that the nearest downdip tremor event in time occurs after the HYSB1 tremor detection.* ***(a)*** *Timing for all 47 validated tremor detections at HYSB1, which shows a peak at -10 days. This peak consists primarily of detections made within the sustained tremor episode on 2017-09-06, which is nearest to a single downdip tremor detection on 2017-09-16.* ***(b)*** *Same as (a) but excluding detections made on 2017-09-06. The nearly flat distribution shows there is no clear timing relationship between HYSB1 tremor and downdip events.*

255

On time	Off time
2015-10-21T07:10:23.104526Z	2015-10-21T07:12:23.118416Z
2016-01-10T21:12:28.952425Z	2016-01-10T21:13:08.957055Z
2016-02-27T12:03:06.156194Z	2016-02-27T12:03:56.163129Z
2016-06-04T14:36:16.200949Z	2016-06-04T14:37:16.207894Z
2016-06-04T14:37:36.210210Z	2016-06-04T14:38:36.217155Z
2016-08-05T16:32:07.005440Z	2016-08-05T16:34:37.022804Z
2016-08-14T00:35:30.362310Z	2016-08-14T00:36:10.366941Z
2016-08-14T14:38:36.217155Z	2016-08-14T14:39:46.225258Z
2016-09-01T15:43:16.666281Z	2016-09-01T15:43:56.670911Z
2016-09-17T02:04:20.979280Z	2016-09-17T02:05:10.985068Z
2016-09-17T02:08:11.005903Z	2016-09-17T02:10:11.019794Z
2016-09-24T18:19:27.750897Z	2016-09-24T18:20:27.757842Z
2016-09-25T03:22:01.518694Z	2016-09-25T03:23:51.531427Z
2016-09-25T03:24:51.538372Z	2016-09-25T03:25:41.544160Z
2016-10-02T12:07:35.168422Z	2016-10-02T12:08:35.175368Z
2016-11-18T05:22:02.352124Z	2016-11-18T05:22:42.356754Z
2017-07-29T04:03:41.808080Z	2017-07-29T04:04:21.812710Z
2017-09-06T10:28:44.482000Z	2017-09-06T10:41:34.571131Z
2017-09-06T13:01:05.539993Z	2017-09-06T13:02:15.548096Z
2017-09-06T13:13:25.625651Z	2017-09-06T13:14:45.634911Z
2017-09-06T13:19:15.666165Z	2017-09-06T13:25:45.711309Z
2017-09-06T13:48:05.866420Z	2017-09-06T13:48:55.872207Z
2017-09-06T13:55:55.920824Z	2017-09-06T13:56:55.927769Z
2017-09-06T13:58:15.937030Z	2017-09-06T14:01:25.959023Z
2017-09-06T14:06:35.994907Z	2017-09-06T14:08:26.007640Z
2017-09-06T14:10:56.025003Z	2017-09-06T14:12:06.033106Z
2017-09-06T14:31:06.165065Z	2017-09-06T14:32:06.172011Z
2017-09-06T14:47:16.277347Z	2017-09-06T14:48:26.285450Z
2017-09-06T15:14:26.466026Z	2017-09-06T15:14:56.469499Z
2017-09-06T15:32:06.588726Z	2017-09-06T15:35:36.613034Z
2017-09-06T16:52:17.145503Z	2017-09-06T16:59:27.195277Z
2017-09-06T17:02:57.219586Z	2017-09-06T17:04:07.227688Z
2017-09-06T17:04:37.231161Z	2017-09-06T17:05:47.239264Z
2017-09-06T17:06:47.246209Z	2017-09-06T17:08:07.255469Z
2017-09-06T17:37:27.459197Z	2017-09-06T17:44:07.505498Z
2018-01-03T15:22:06.519273Z	2018-01-03T15:22:46.523903Z
2018-02-10T14:43:16.249566Z	2018-02-10T14:43:56.254196Z
2018-03-13T15:48:13.129559Z	2018-03-13T15:48:53.136904Z
2018-03-15T00:03:50.142378Z	2018-03-15T00:05:00.150480Z
2018-06-26T12:51:25.472856Z	2018-06-26T12:52:15.478643Z
2018-06-26T13:01:05.539993Z	2018-06-26T13:09:55.601343Z
2018-09-19T07:27:03.220280Z	2018-09-19T07:28:43.231856Z
2019-07-11T03:20:01.897256Z	2019-07-11T03:21:01.906013Z

2019-07-11T03:32:32.006713Z	2019-07-11T03:33:22.014011Z
2019-07-11T03:46:02.124927Z	2019-07-11T03:47:02.133684Z
2022-08-21T18:37:17.874754Z	2022-08-21T18:38:37.884014Z
2023-01-29T16:30:26.993865Z	2023-01-29T16:31:47.003125Z

Table S3. *On and off trigger times of all visually verified tremor detections at station HYSB1 (Figure 6a).*

Date	Time
2015-10-21	04:25 – 07:25
2016-06-04	14:15 - 16:45*
2017-09-06	10:30 – 17:50
2018-06-26	12:25 – 13:35

Table S4. *Time periods of observed long-duration tremor on the Slope Base station (HYSB1). *A data outage begins starting at 16:45 that persists until 18:45. When the data comes back online at 18:45, tremor has subsided.*